Matrix Isolation Infrared Spectroscopic and Theoretical Studies on the Reactions of Niobium and Tantalum Mono- and Dioxides with Methane

Guanjun Wang, Sixue Lai, Mohua Chen, and Mingfei Zhou*

Department of Chemistry & Laser Chemistry Institute, Shanghai Key Laboratory of Molecular Catalysts and Innovative Materials, Fudan University, Shanghai 200433, People's Republic of China

Received: July 5, 2005; In Final Form: August 25, 2005

The reactions of niobium and tantalum monoxides and dioxides with methane have been investigated using matrix isolation infrared spectroscopic and theoretical calculations. The niobium and tantalum oxide molecules were prepared by laser evaporation of Nb_2O_5 and Ta_2O_5 bulk targets. The niobium monoxide molecule interacted with methane to form the $ONb(CH_4)$ complex, which was predicted to have C_{3v} symmetry with the metal atom coordinated to three hydrogen atoms of the methane molecule. The $ONb(CH_4)$ complex rearranged to the $CH_3Nb(O)H$ isomer upon 300 nm $< \lambda <$ 580 nm irradiation. The analogous $OTa(CH_4)$ complex was not observed, but the $CH_3Ta(O)H$ molecule was produced upon UV irradiation. The niobium and tantalum dioxide molecules reacted with methane to form the $O_2Nb(CH_4)$ and $O_2Ta(CH_4)$ complexes with C_s symmetry, which underwent photochemical rearrangement to the $CH_3Nb(O)OH$ and $CH_3Ta(O)OH$ isomers upon ultraviolet irradiation.

Introduction

The controlled partial oxidation of methane to produce chemical feedstocks such as methanol is of great economic and scientific importance. A variety of transition metal oxide containing catalyst systems were developed upon catalytic conversion of methane to methanol. The reactions of transition metal oxide molecules with methane may serve as the simplest model for understanding the intrinsic mechanism of the catalytic conversion processes. The gas phase reactions of transition metal oxide ions with methane have been studied both experimentally and theoretically.[1−6] Schröder, Schwarz, and co-workers have systematically investigated the gas phase reactions of the first row transition metal monoxide ions and methane, demonstrating that late transition metal monoxide ions can efficiently convert methane to methanol, while the early transition metal monoxide ions cannot.[1] Yoshizawa and co-workers have calculated the reaction pathway and energetics for methane-to-methanol conversion by first row transition metal monoxide ions.[5] The $MO^+ + CH_4 \rightarrow M^+ + CH_3OH$ reactions were suggested to proceed via the initial formation of a $OM^+(CH_4)$ complex followed by the isomerization to the HOM^+CH_3 and $M^+(CH_3OH)$ intermediates via two transition states. The results showed that the experimentally observed reaction efficiency and methanol-to-methyl branching ratio could be rationalized in terms of the predicted barrier heights at the transition states. The reactivities of different iron-oxo species FeO^{n+} ($n = 0, 1, 2$) toward methane were also computed by Yoshizawa et al., and it was found that the iron(IV)-oxo species are most effective for the cleavage of the C−H bond of methane.[6]

The reactions of neutral transition metal oxides with methane have received much less attention. However, the interactions of neutral metal monoxide with methane have been theoretically studied. Density functional theoretical investigations found that palladium monoxide can form a weak complex with methane. The insertion of PdO into the C−H bond of methane to form CH_3PdOH was predicted to have an energy barrier of 24.5 kcal/mol.[7,8] The reactions of scandium, nickel, and palladium monoxides with methane were also studied by Hwang and Mebel using density functional calculations.[9,10] The results showed that neutral NiO and PdO are reactive toward methane and can form molecular complexes with CH_4 bound by 8−9 kcal/mol, whereas ScO is not reactive with respect to methane at low and ambient temperatures. Goddard and co-workers investigated methane activation by MO_x (M = Cr, Mo, W; $x =$ 1, 2, 3) and found that the trends in reactivity can be rationalized in terms of changes in the electrophilicity of MO_x, the strength of the M−O π bonds, and the binding properties of MO_x to methyl or hydrogen.[11] These theoretical studies have provided valuable information concerning the reaction mechanism and energetics.

Recently, we have investigated the reactions of iron and manganese monoxide molecules with methane using matrix isolation infrared absorption spectroscopy as well as theoretical calculations.[12] It was found that the ground state iron and manganese monoxide molecules reacted spontaneously with methane to form the weakly bound $OM(CH_4)$ (M = Fe, Mn) complexes, which rearranged to the inserted CH_3MOH molecules under ultraviolet irradiation. The calculation results also showed that the reaction path $MO + CH_4 \rightarrow OM(CH_4) \rightarrow TS1 \rightarrow CH_3MOH \rightarrow TS2 \rightarrow M(CH_3OH) \rightarrow M + CH_3OH$ does not require spin crossing, which is quite different from the corresponding $MO^+ + CH_4$ reactions. In this paper, we report a combined matrix isolation infrared spectroscopic and theoretical study of the reactions of niobium and tantalum mono- and dioxides with methane.

Experimental and Theoretical Methods

The experimental setup for pulsed laser evaporation and matrix isolation Fourier transform infrared (FTIR) spectroscopic investigation has been described in detail previously.[13] Briefly, the 1064 nm Nd:YAG laser fundamental (Spectra Physics, DCR 150, 20 Hz repetition rate and 8 ns pulse width) was focused

* Corresponding author. E-mail: mfzhou@fudan.edu.cn.

10.1021/jp053666u CCC: $30.25
Published on Web 10/05/2005

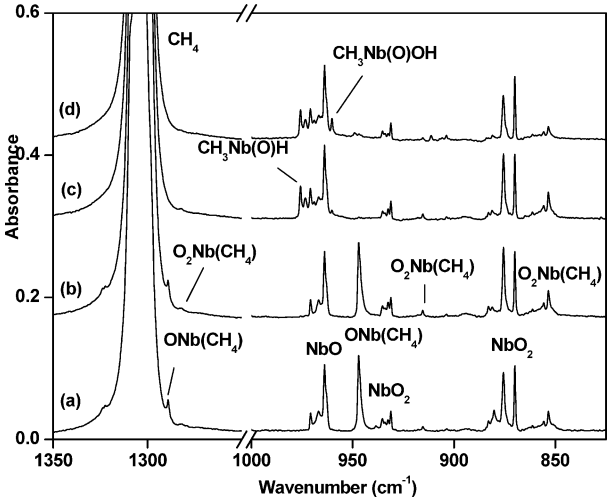

Figure 1. Infrared spectra in the 1350−1250 and 1000−825 cm^{-1} regions from the codeposition of laser-evaporated niobium oxides with 1.0% CH_4 in argon: (a) after 2 h of sample deposition at 12 K; (b) after 30 K annealing; (c) after 30 min of 300 nm < λ < 580 nm irradiation; (d) after 30 min of 250 nm < λ < 580 nm irradiation.

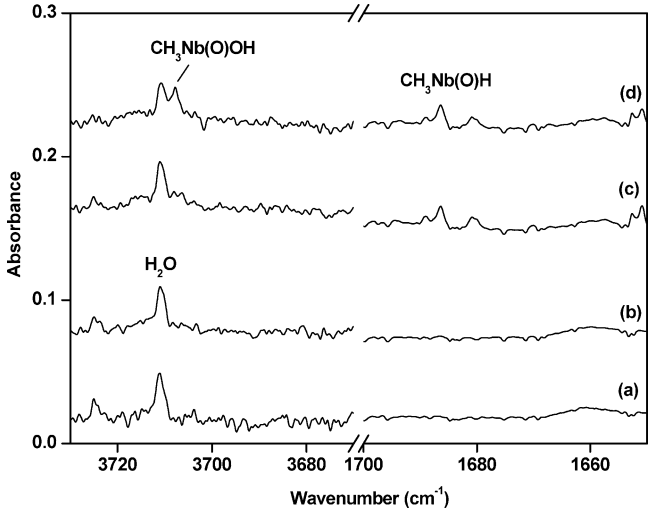

Figure 2. Infrared spectra in the 3730−3670 and 1700−1650 cm^{-1} regions from the codeposition of laser-evaporated niobium oxides with 1.0% CH_4 in argon: (a) after 2 h of sample deposition at 12 K; (b) after 30 K annealing; (c) after 30 min of 300 nm < λ < 580 nm irradiation; (d) after 30 min of 250 nm < λ < 580 nm irradiation.

onto the rotating Nb_2O_5 or Ta_2O_5 targets, which were prepared by sintered metal oxide powders. The ablated species were codeposited with methane in excess argon onto a 12 K CsI window for 2 h at a rate of approximately 2−4 mmol/h. Isotopically labeled CD_4 (Isotec, 99%), $^{13}CH_4$ (Isotec, 99%), and mixtures were used in different experiments. Infrared spectra were recorded on a Bruker IFS 113 V spectrometer at a 0.5 cm^{-1} resolution using a DTGS detector. Matrix samples were annealed at different temperatures, and selected samples were subjected to broad-band irradiation using a 250 W high-pressure mercury arc lamp and glass filters.

Density functional calculations were performed using the Gaussian 03 program.[14] The three-parameter hybrid functional according to Becke with additional correlation corrections due to Lee, Yang, and Parr (B3LYP) was utilized.[15] Additional comparison calculations on the weakly bound $OM(CH_4)$ complexes were also done using the B3PW91 functionals.[16] The 6-311++G** basis set for H, C, and O atoms and the SDD pseudopotential and basis set for Nb and Ta were used.[17,18] The

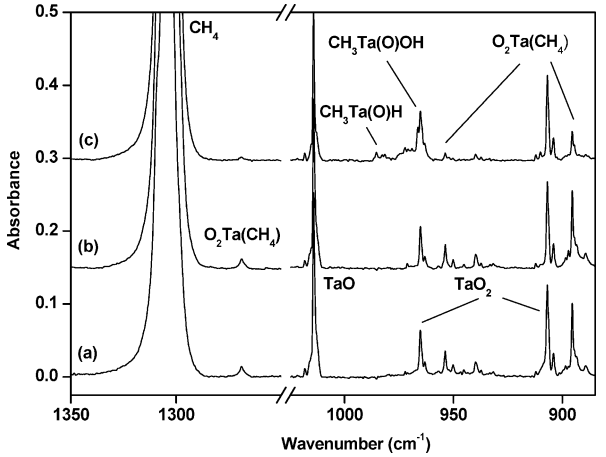

Figure 3. Infrared spectra in the 1350−1250 and 1025−885 cm^{-1} regions from the codeposition of laser-evaporated tantalum oxides with 1.0% CH_4 in argon: (a) after 2 h of sample deposition at 12 K; (b) after 30 K annealing; (c) after 30 min of 250 nm < λ < 580 nm irradiation.

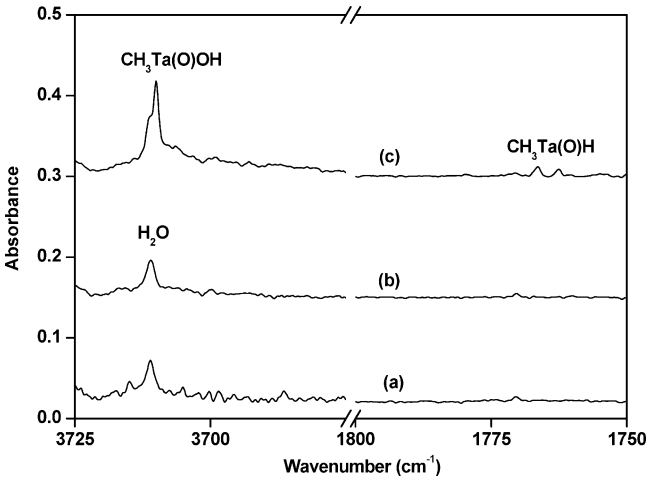

Figure 4. Infrared spectra in the 3725−3675 and 1800−1750 cm^{-1} regions from the codeposition of laser-evaporated tantalum oxides with 1.0% CH_4 in argon: (a) after 2 h of sample deposition at 12 K; (b) after 30 K annealing; (c) after 30 min of 250 nm < λ < 580 nm irradiation.

geometries were fully optimized, and the stability of the electronic wave function was tested; the harmonic vibrational frequencies were calculated with analytic second derivatives, and zero point energies (ZPEs) were derived. The single point energies of all of the structures optimized at the B3LYP level were calculated using the CCSD(T) method with the same basis sets.[19]

Results and Discussion

Infrared Spectra. The niobium and tantalum oxides were produced by laser evaporation of the bulk Nb_2O_5 and Ta_2O_5 targets. Codeposition of laser-evaporated niobium and tantalum oxides with pure argon at 12 K forms monoxides (NbO, 963.9 cm^{-1}; TaO, 1014.3 cm^{-1}) and dioxides (NbO_2, 931.2 and 869.9 cm^{-1}; TaO_2, 907.0 and 965.3 cm^{-1}) as the major products. These niobium and tantalum oxide species have previously been identified from the effects of isotopic substitution in their infrared spectra and from comparison to frequencies calculated by using density functional theory.[20−22]

New absorptions were observed when laser-evaporated niobium and tantalum oxide molecules were codeposited with

TABLE 1: Infrared Absorptions (cm^{-1}) from the Codeposition of Laser-Evaporated Niobium and Tantalum Oxides with CH_4 in Solid Argon (For Comparison, the Calculated Isotopic Frequencies (cm^{-1}) Are Listed in Parentheses)

CH_4	$^{13}CH_4$	CD_4	assignment
963.9			NbO
931.2			NbO_2 (ν_1)
875.5			NbO_2 (ν_3 site)
869.9			NbO_2 (ν_3)
1289.1 (1327.1)	1281.5 (1281.5)	(1003.8)	$ONb(CH_4)$ (CH_2 deformation)
947.1 (977.7)	947.1 (977.7)	944.1 (976.4)	$ONb(CH_4)$ (Nb−O stretch)
1686.6 (1780.9)	1686.6 (1780.9)	1212.3 (1267.3)	$CH_3Nb(O)H$ (Nb−H stretch)
975.8 (992.8)	975.5 (992.7)	975.6 (991.3)	$CH_3Nb(O)H$ (Nb−O stretch)
1282.0 (1301.9)	1274.9 (1294.2)	(985.0)	$O_2Nb(CH_4)$ (CH_2 deformation)
915.5 (953.0)	915.5 (953.0)	915.1 (950.4)	$O_2Nb(CH_4)$ (Nb−O sym. stretch)
853.4 (908.7)	853.4 (908.7)	853.2 (908.4)	$O_2Nb(CH_4)$ (Nb−O asym. stretch)
3707.8 (3909.6)	3707.8 (3909.6)	2735.0 (2848.2)	$CH_3Nb(O)OH$ (O−H stretch)
960.5 (974.0)	960.1 (973.9)	960.5 (973.6)	$CH_3Nb(O)OH$ (Nb−O stretch)
1014.3			TaO
965.3			TaO_2 (ν_1)
907.0			TaO_2 (ν_3)
1766.6 (1829.2)	1766.6 (1929.2)	1265.9 (1298.1)	$CH_3Ta(O)H$ (Ta−H stretch)
1160.8 (1204.2)	(1194.3)	915.9 (946.4)	$CH_3Ta(O)H$ (CH_2 deformation)
974.7 (975.1)	974.7 (975.0)	974.0 (972.9)	$CH_3Ta(O)H$ (Ta−O stretch)
1268.9 (1299.0)	1261.6 (1291.2)	(983.0)	$O_2Ta(CH_4)$ (CH_2 deformation)
953.8 (953.8)	953.8 (953.8)	949.9 (951.2)	$O_2Ta(CH_4)$ (Ta−O sym. stretch)
895.5 (904.6)	895.5 (904.6)	895.4 (904.5)	$O_2Ta(CH_4)$ (Ta−O asym. stretch)
3709.9 (3916.4)	3709.9 (3916.4)	2737.3 (2853.5)	$CH_3Ta(O)OH$ (O−H stretch)
966.5 (957.7)	966.4 (957.6)	966.0 (957.0)	$CH_3Ta(O)OH$ (Ta−O stretch)
692.0 (692.1)	(691.4)	681.3 (664.9)	$CH_3Ta(O)OH$ (Ta−OH) stretch

methane in excess argon. The spectra in select regions are shown in Figures 1−4, and the frequencies are listed in Table 1. On the basis of their growth/decay characteristics measured as a function of changes of experimental conditions, the new product absorptions can be classified into several groups. In the case of niobium, the band set at 1289.1 and 947.1 cm^{-1} was observed upon sample deposition (Figure 1, trace a), was kept almost unchanged upon annealing (Figure 1, trace b), and disappeared when the matrix was irradiated by the output of the high-pressure mercury arc lamp with a $\lambda > 300$ nm pass filter (300 nm $< \lambda <$ 580 nm, Figure 1, trace c). The band set at 1282.0, 915.1, and 853.2 cm^{-1} also was observed after sample deposition, increased slightly upon annealing, and showed no obvious change upon 300 nm $< \lambda <$ 580 nm irradiation, but it decreased significantly upon 250 nm $< \lambda <$ 580 nm irradiation (Figure 1, trace d). A pair of new bands at 1686.6 and 975.8 cm^{-1} appeared upon 300 nm $< \lambda <$ 580 nm irradiation (Figures 1 and 2, trace c), and two new bands at 3707.8 and 960.5 cm^{-1} were produced under 250 nm $< \lambda <$ 580 nm irradiation (Figures 1 and 2, trace d).

In the reaction of laser-evaporated tantalum oxides with methane, new absorptions at 1268.9, 953.8, and 895.5 cm^{-1} were observed after sample deposition (Figure 3, trace a), increased upon annealing (Figure 3, trace b), and decreased significantly upon 250 nm $< \lambda <$ 580 nm irradiation (Figure 3, trace c). New absorptions at 1766.6, 1160.8, 974.7, 3709.9, 966.5, and 692.0 cm^{-1} were produced upon broad-band irradiation as well (Figures 3 and 4, trace c).

The experiments were repeated with the isotopic substituted CD_4 and $^{13}CH_4$ samples. The isotope frequencies are also listed in Table 1. The infrared spectra in selected regions using different isotopic samples are shown in Figures 5−8, respectively.

Calculation Results. Quantum chemical calculations were performed on the potential product molecules. The optimized structures are shown in Figures 9 and 10. The vibrational frequencies and intensities of various species involved in the niobium and tantalum oxides and methane reaction systems are listed in Tables 2 and 3, respectively.

$OM(CH_4)$. The absorptions at 1289.1 and 947.1 cm^{-1} in the niobium experiments are due to different vibrational modes of the same species. The 1289.1 cm^{-1} band shifted to 1281.5 cm^{-1} with $^{13}CH_4$. The $^{12}C/^{13}C$ isotopic frequency ratio of 1.0059 is very close to that of the CH_2 deformation mode of CH_4 observed at 1305.4 cm^{-1} in solid argon. The band position and isotopic frequency shift suggest the assignment of the 1289.1 cm^{-1} band to the CH_2 deformation mode of a CH_4 complex. The 947.1 cm^{-1} band is 16.8 cm^{-1} lower than the frequency of NbO in solid argon and is in the spectral range expected for the terminal Nb−O stretching mode of a NbO complex. This band showed no shift with the $^{13}CH_4$ sample and shifted to 944.1 cm^{-1} with the CD_4 sample. The spectral feature in the experiment with the mixture of CH_4 and CD_4 (Figure 5, trace b) implies that only one CH_4 subunit is involved in the species. These experimental observations lead us to assign the 1289.1 and 947.1 cm^{-1} bands to the CH_2 deformation and Nb−O stretching vibrations of the $ONb(CH_4)$ complex.

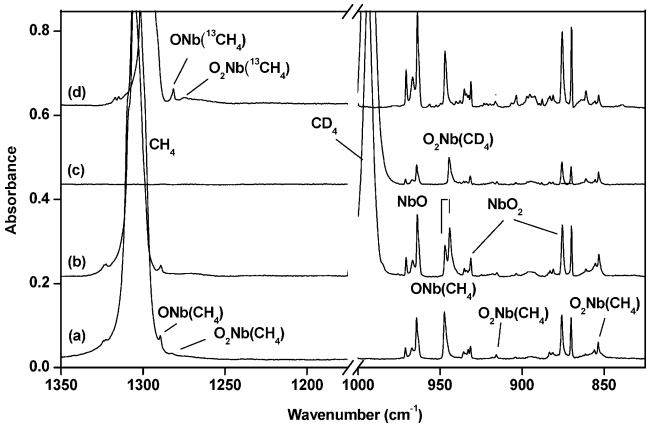

Figure 5. Infrared spectra in the 1350−1175 and 1000−825 cm^{-1} regions from the codeposition of laser-evaporated niobium oxides with methane in excess argon. Spectra were taken after 2 h of sample deposition followed by 30 K annealing: (a) 1.0% CH_4; (b) 0.5% CH_4 + 0.5% CD_4; (c) 1.0% CD_4; (d) 1.0% $^{13}CH_4$.

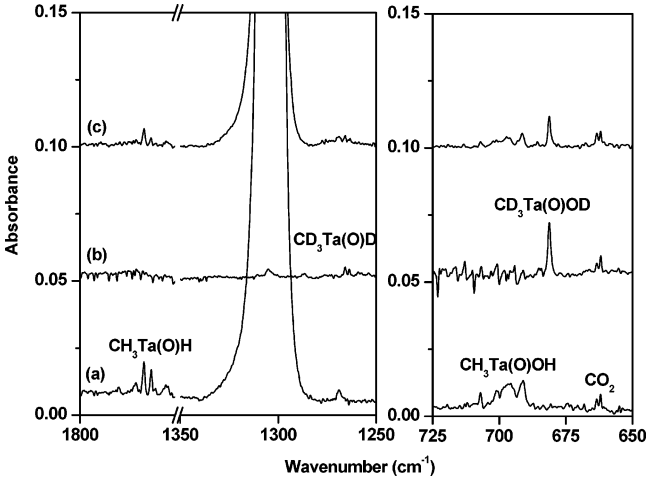

Figure 6. Infrared spectra in the 1800−1750 and 725−650 cm^{-1} regions from the codeposition of laser-evaporated tantalum oxides with methane in excess argon. Spectra were taken after 2 h of sample deposition followed by 30 min of broad-band irradiation: (a) 1.0% CH_4; (b) 1.0% CD_4; (c) 0.5% CH_4 + 0.5% CD_4.

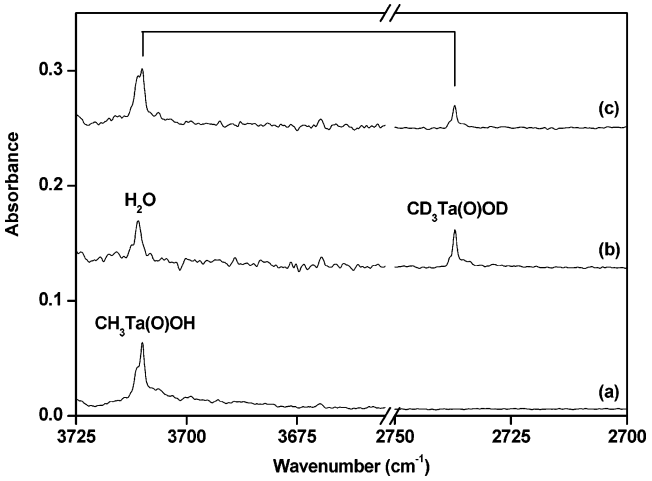

Figure 7. Infrared spectra in the 3725−3650 and 2750−2700 cm^{-1} regions from the codeposition of laser-evaporated tantalum oxides with methane in excess argon. Spectra were taken after 2 h of sample deposition followed by 30 min of broad-band irradiation: (a) 1.0% CH_4; (b) 1.0% CD_4; (c) 0.5% CH_4 + 0.5% CD_4.

Density functional calculations indicated that the $ONb(CH_4)$ complex has a $^4A_1$ ground state with C_{3v} symmetry (Figure 9). The niobium atom of NbO is coordinated to three hydrogen atoms of CH_4, that is, η^3-CH_4 bonding. The $^4A_1$ state correlates to the ground state NbO ($^4\Sigma^-$) and CH_4 and is very weakly bound.[20,23] The distance between Nb and H is 3.506 Å at the B3LYP/6-311++G**/SDD level and 3.056 Å at the B3PW91/6-311++G**/SDD level. The binding energy of $ONb(CH_4)$ was predicted to be only 0.9 kcal/mol with respect to NbO ($^4\Sigma^-$) + CH_4 calculated at the CCSD(T)/B3LYP/6-311++G**/SDD level. The calculations predicted that the CH_2 deformation and Nb−O stretching modes have the highest IR intensities. The CH_2 deformation mode of the complex predicted at 1327.1 cm^{-1} is red-shifted about 13.2 cm^{-1} from that of free CH_4, and the Nb−O stretching mode at 977.7 cm^{-1} is red-shifted by 5.6 cm^{-1} from that of the ground state NbO ($^4\Sigma^-$), which are in reasonable agreement with the experimental values. Another CH_2 deformation mode predicted at 1345.6 cm^{-1} with appreciable IR intensity was overlapped by the strong CH_4 absorption predicted at 1340.3 cm^{-1} (experimentally observed at 1305.4 cm^{-1}).

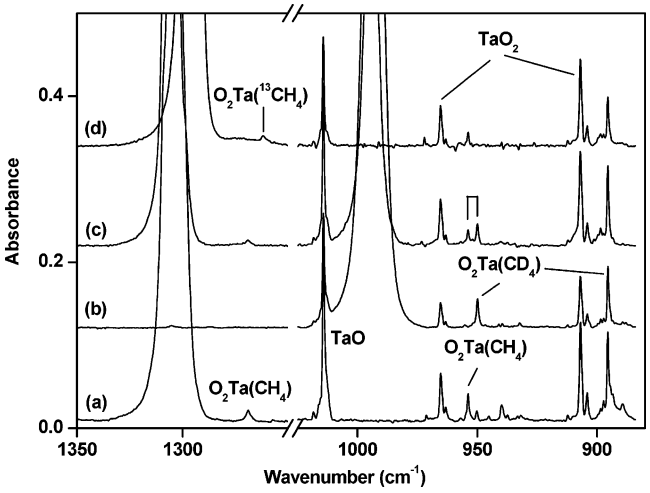

Figure 8. Infrared spectra in the 1350−1250 and 1025−880 cm^{-1} regions from the codeposition of laser-evaporated tantalum oxides with methane in excess argon. Spectra were taken after 2 h of sample deposition followed by 30 K annealing: (a) 1.0% CH_4; (b) 1.0% CD_4; (c) 0.5% CH_4 + 0.5% CD_4; (d) 1.0% $^{13}CH_4$.

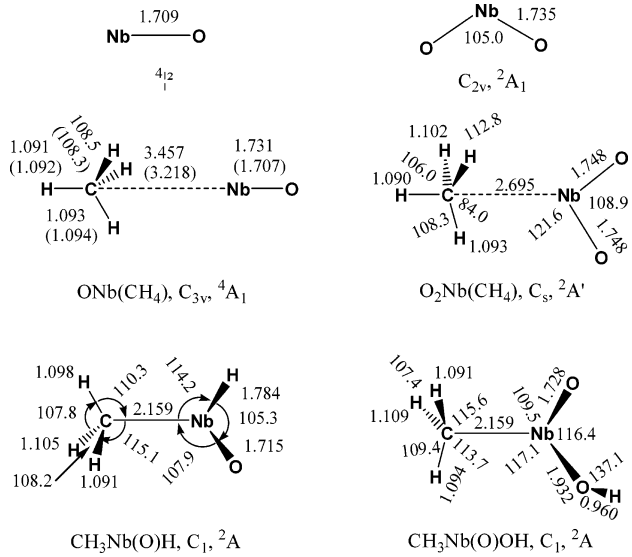

Figure 9. Optimized structures (bond lengths in angstroms, bond angles in degrees) of the species observed in the niobium system at the B3LYP/6-311++G**/SDD and B3PW91/6-311++G**/SDD (values in parentheses) levels of theory.

No absorptions can be assigned to the analogous $OTa(CH_4)$ complex. In contrast to NbO, which has a quartet ground state, the TaO molecule has a doublet ($^2\Delta$) ground state.[20,22] The ground state TaO molecule interacts with methane to form the $OTa(CH_4)$ complex, which was predicted to have a ^2E ground state with C_{3v} symmetry (Figure 10). This complex is very weakly bound, having a binding energy of only 1.0 kcal/mol with respect to the ground state TaO ($^2\Delta$) and CH_4 at the CCSD-(T)/B3LYP/6-311++G**/SDD level. The CH_2 deformation and Ta−O stretching modes of the complex were computed at 1345.3, 1335.3, and 1009.1 cm^{-1}, respectively. We assume that the $OTa(CH_4)$ complex was formed in the present experiments, and its absorptions are most probably overlapped by the strong CH_4 (predicted at 1340.3 cm^{-1}) and TaO (predicted at 1008.7 cm^{-1}) absorptions.

$CH_3M(O)H$. The band set at 1686.6 and 975.8 cm^{-1} was produced under 300 nm < λ < 580 nm irradiation. The band at 1686.6 cm^{-1} showed no shift with the $^{13}CH_4$ sample and shifted to 1212.3 cm^{-1} with the CD_4 sample. The band position and

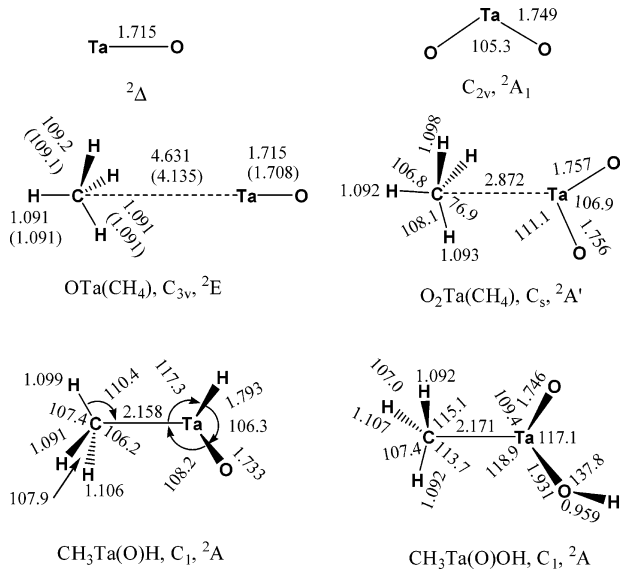

Figure 10. Optimized structures (bond lengths in angstroms, bond angles in degrees) of the species observed in the tantalum system at the B3LYP/6-311++G**/SDD and B3PW91/6-311++G**/SDD (values in parentheses) levels of theory.

the H/D isotope frequency ratio (1.3912) are characteristic of a Nb−H stretching vibration, which are very close to those of the Nb−H stretching mode of HNbOH (1587.5 cm^{-1} with a H/D ratio of 1.3911).[24] The 975.8 cm^{-1} band exhibited only 0.3 and 0.2 cm^{-1} shifts when the $^{13}CH_4$ and CD_4 samples were employed and is suggestive of a Nb−O stretching vibration. Note that the 1686.6 and 975.8 cm^{-1} bands were produced only upon 300 nm < λ < 580 nm irradiation, during which the ONb-(CH_4) absorptions were destroyed. This suggests that the 1686.6 and 975.8 cm^{-1} bands are most likely due to another structural isomer of ONb(CH_4). Accordingly, we assign the 1686.6 and 975.8 cm^{-1} bands to the Nb−H and Nb−O stretching modes of $CH_3Nb(O)H$, which was predicted to have a doublet ground state without any symmetry (Figure 9). As listed in Table 2, the Nb−H and Nb−O stretching modes were computed at 1780.9 and 992.8 cm^{-1}, respectively, in good agreement with the observed values. The calculated isotopic frequency shifts (Table 1) also fit the experimental values.

Similarly, absorptions at 1766.6, 974.7, and 1160.8 cm^{-1} in the tantalum system are assigned to the $CH_3Ta(O)H$ molecule. The 1766.6 cm^{-1} band is due to the Ta−H stretching mode, which was observed at 1265.9 cm^{-1} with the CD_4 sample. The 974.7 cm^{-1} band is assigned to the Ta−O stretching mode, which is red-shifted 39.6 cm^{-1} from that of TaO. The 1160.8 cm^{-1} band is weak and is assigned to the CH_2 deformation mode. The deuterium counterpart was observed at 915.9 cm^{-1}. The experimentally observed modes were computed at 1829.2, 975.1, and 1204.2 cm^{-1}, respectively, for the doublet ground state $CH_3Ta(O)H$ molecule (Figure 10).

$O_2M(CH_4)$. The absorptions at 1282.0, 915.5, and 853.4 cm^{-1} were assigned to the niobium dioxide−methane complex, O_2-Nb(CH_4). The 853.4 and 915.5 cm^{-1} bands are appropriate for the antisymmetric and symmetric ONbO stretching vibrations. These bands are 16.5 and 15.7 cm^{-1} lower than the corresponding modes of NbO_2 in solid argon.[20] Both bands showed no shift with $^{13}CH_4$ and very small shifts (0.2 and 0.4 cm^{-1}) with CD_4. The very weak 1282.0 cm^{-1} band is due to the CH_2 deformation mode of the complex, which shifted to 1274.9 cm^{-1} with $^{13}CH_4$. Density functional calculations predicted that the $O_2Nb(CH_4)$ complex has a $^2A'$ ground state with C_s symmetry, as shown in Figure 9. The three experimentally observed modes were calculated at 1301.9, 953.0, and 908.7 cm^{-1} and agree well with the experimental values.

The absorptions at 1268.9, 953.8, and 895.5 cm^{-1} in the tantalum system are assigned to the analogous $O_2Ta(CH_4)$ complex. The 953.8 and 895.5 cm^{-1} bands are due to symmetric and antisymmetric OTaO stretching modes, which both red-shifted by 11.5 cm^{-1} from those of TaO_2 in solid argon. The 1268.9 cm^{-1} band is due to the CH_2 deformation mode of the complex. These three modes were calculated at 1297.4, 973.2, and 918.3 cm^{-1} for the $^2A'$ ground state $O_2Ta(CH_4)$ complex.

$CH_3M(O)OH$. The bands at 3707.8 and 960.5 cm^{-1} are assigned to the $CH_3Nb(O)OH$ molecule. These bands appeared together only upon broad-band irradiation during which the O_2-Nb(CH_4) absorptions disappeared. The 3707.8 cm^{-1} band is in the frequency region expected for an O−H stretching vibration. It shifted to 2735.0 cm^{-1} with the CD_4 sample, giving a H/D ratio of 1.3557, which is characteristic of an O−H stretching vibration. The band at 960.5 cm^{-1} exhibited a very small shift (0.4 cm^{-1}) with the $^{13}CH_4$ sample and no shift with the CD_4 sample and is appropriate for a Nb−O stretching mode. The $CH_3Nb(O)OH$ molecule was predicted to have a doublet ground state (Figure 9) with C_1 symmetry. The O−H and Nb−O stretching modes were computed at 3909.6 and 974.0 cm^{-1}, respectively, with the calculated isotopic frequency shifts (Table 1) in good agreement with the experimental values.

Similarly, the absorptions at 3709.9, 966.5, and 692.0 cm^{-1} in the tantalum system are assigned to the $CH_3Ta(O)OH$ molecule. The 3709.9 cm^{-1} band shifted to 2737.3 cm^{-1} with CD_4 and is due to the O−H stretching vibration. The terminal Ta−O stretching mode is observed at 966.5 cm^{-1}, and it shifted to 966.4 and 966.1 cm^{-1} when the $^{13}CH_4$ and CD_4 samples were employed. The absorption at 692.0 cm^{-1} is weak and broad and is assigned to the Ta−OH stretching mode. This mode became sharp and was observed at 681.3 cm^{-1} when CD_4 was used. The broad feature observed in the normal experiments suggests that this mode is in Fermi resonance with low-lying levels. The O−H, Ta−O, and Ta−OH stretching modes of the doublet ground state $CH_3Ta(O)OH$ molecule (Figure 10) were predicted to be 3916.4, 957.7, and 692.1 cm^{-1}, respectively.

Reaction Mechanism. Laser evaporation of the Nb_2O_5 and Ta_2O_5 targets produces metal monoxides (NbO and TaO) and metal dioxides (NbO_2 and TaO_2) as the major products. The OM(CH_4) and $O_2M(CH_4)$ (M = Nb, Ta) complexes were formed by the reactions of metal mono- and dioxides with CH_4 molecules, reactions 1−4, which were predicted to be exothermic at the CCSD(T)/B3LYP/6-311++G**/SDD level.

$$NbO\ (^4\Sigma^-) + CH_4 \rightarrow ONb(CH_4)\ (^4A_1) \qquad \Delta E = -0.9\ \text{kcal/mol} \quad (1)$$

$$TaO\ (^2\Delta) + CH_4 \rightarrow OTa(CH_4)\ (^2E) \qquad \Delta E = -1.0\ \text{kcal/mol} \quad (2)$$

$$NbO_2\ (^2A_1) + CH_4 \rightarrow O_2Nb(CH_4)\ (^2A') \qquad \Delta E = -7.4\ \text{kcal/mol} \quad (3)$$

$$TaO_2\ (^2A_1) + CH_4 \rightarrow O_2Ta(CH_4)\ (^2A') \qquad \Delta E = -4.9\ \text{kcal/mol} \quad (4)$$

The binding energies of 7.4 and 4.9 kcal/mol for NbO_2 and TaO_2 are significantly larger than those for the corresponding monoxides (NbO, 0.9 kcal/mol; TaO, 1.0 kcal/mol). The trend is the same as that of group VI (Cr, Mo, W) metal oxides. Xu et al. found that the binding energies of high oxidative complexes $O_xM(CH_4)$ (M = Cr, Mo, W; x = 1, 2, 3) are larger

TABLE 2: Total Energies (in Hartrees, after Zero Point Energy Correction), Vibrational Frequencies (cm^{-1}), and Intensities (km/mol) of Various Species in the $Nb_2O_5 + CH_4$ System Calculated at the B3LYP/6-311++G/SDD Level of Theory**

	E_{tot}	frequency (intensity, mode)
CH_4 ($^1A_1$)	−40.489 422	1340.3 (54, t_2), 1558.5 (0, e), 3024.1 (0, a_1), 3129.7 (78, t_2)
NbO ($^4\Sigma^-$)	−132.179 803	983.3 (161, σ)
NbO_2 ($^2A_1$)	−207.493 430	344.5 (1, a_1), 927.8 (238, b_2), 973.1 (118, a_1)
$ONb(CH_4)$ ($^4A_1$)	−172.669 116	24.7 (3, a_1), 42.7 (22, e), 100.3 (0, e), 977.7 (195, a_1), 1327.1 (57, a_1), 1345.6 (40, e), 1556.3 (24, e), 3011.1 (6, a_1), 3115.3 (12, e), 3124.0 (38, a_1)
$O_2Nb(CH_4)$ ($^2A'$)	−247.988 970	13.0 (12, a″), 51.8 (3, a′), 74.8 (4, a″), 131.8 (1, a′), 159.0 (4, a′), 324.1 (6, a′), 330.8 (1, a″), 908.7 (284, a′), 953.0 (98, a′), 1301.9 (50, a′), 1339.3 (17, a′), 1370.9 (39, a″), 1547.6 (50, a″), 1555.7 (13, a′), 2921.5 (21, a′), 3013.9 (0, a″), 3095.2 (0, a′), 3134.3 (1, a′)
$CH_3Nb(O)H$ (^2A)	−172.706 603	113.3 (1), 202.5 (6), 340.3 (47), 471.1 (24), 531.7 (46), 598.9 (5), 621.9 (60), 992.8 (181), 1186.0 (6), 1408.2 (6), 1430.7 (7), 1780.9 (294), 2941.5 (8), 3035.6 (5), 3119.2 (3)
$CH_3Nb(O)OH$ (^2A)	−248.027 051	102.8 (0), 133.8 (1), 168.2 (3), 219.6 (9), 390.2 (93), 397.8 (48), 528.8 (155), 568.0 (40), 593.1 (6), 695.8 (111), 974.0 (185), 1189.7 (13), 1407.4 (5), 1433.6 (7), 2919.2 (8), 3060.7 (5), 3118.5 (3), 3909.6 (217)

TABLE 3: Total Energies (in Hartrees, after Zero Point Energy Correction), Vibrational Frequencies (cm^{-1}), and Intensities (km/mol) of Various Species in the $Nb_2O_5 + CH_4$ System Calculated at the B3LYP/6-311++G/SDD Level of Theory**

	E_{tot}	frequency (intensity, mode)
TaO ($^2\Delta$)	−132.213 694	1008.7 (104, σ)
TaO_2 ($^2A_1$)	−207.540 293	332.9 (17, a_1), 914.8 (193, b_2), 966.5 (60, a_1)
$OTa(CH_4)$ (^2E)	−172.702 875	8.5 (0, a_1), 46.4 (8, e), 65.9 (6, e), 1009.1 (113, a_1), 1335.3 (41, a_1), 1345.3 (38, e), 1558.2 (4, e), 3022.2 (1, a_1), 3127.3 (36, e), 3129.1 (34, a_1)
$O_2Ta(CH_4)$ ($^2A'$)	−248.032 686	38.7 (7, a′), 39.1 (2, a″), 60.2 (17, a″), 103.0 (12, a′), 145.6 (0, a′), 217.0 (0, a″), 322.5 (7, a′), 904.6 (221, a′), 953.8 (86, a′), 1299.0 (65, a′), 1341.5 (19, a′), 1360.8 (33, a″), 1547.2 (28, a″), 1551.1 (13, a′), 2961.3 (40, a′), 3051.9 (0, a″), 3095.7 (4, a′), 3120.5 (4, a′)
$CH_3Ta(O)H$ (^2A)	−172.753 725	112.8 (0), 195.1 (7), 344.1 (19), 466.5 (22), 531.7 (23), 606.8 (5), 658.5 (24), 975.1 (149), 1204.2 (13), 1409.3 (6), 1430.2 (10), 1829.2 (251), 2941.5 (5), 3028.3 (5) 3115.8 (2)
$CH_3Ta(O)OH$ (^2A)	−248.078325	93.8 (0), 117.2 (1), 162.4 (3), 215.9 (10), 412.7 (39), 417.1 (99), 533.7 (166), 564.0 (35), 609.5 (5), 692.1 (83), 957.7 (150), 1207.6 (21), 1411.8 (6), 1433.9 (8), 2936.5 (4), 3057.0 (5), 3110.7 (3), 3916.4 (215)

than those of low oxidative complexes.[11] The binding energies of monoxides (NbO and TaO) are much smaller than those of later transition metal monoxides, such as NiO and PdO (8−9 kcal/mol).[9,10]

The $ONb(CH_4)$ complex absorptions disappeared upon 300 nm < λ < 580 nm irradiation, during which the $CH_3Nb(O)H$ absorptions were produced. This suggests that the $CH_3Nb(O)H$ molecule was generated from the $ONb(CH_4)$ complex via reaction 5:

$$ONb(CH_4)\ (^4A_1) + h\nu \rightarrow CH_3Nb(O)H\ (^2A) \qquad (5)$$

$$OTa(CH_4)\ (^2E) + h\nu \rightarrow CH_3Ta(O)H\ (^2A) \qquad (6)$$

Although the $OTa(CH_4)$ complex absorptions were not observed due to band overlap, the $CH_3Ta(O)H$ absorptions appeared upon broad-band irradiation, indicating that $CH_3Ta(O)H$ was produced via similar photoinduced isomerization reaction 6. Reactions 5 and 6 were predicted to be exothermic by about 27.6 and 29.0 kcal/mol, respectively, at the CCSD(T)/B3LYP/6-311++G**/SDD level.

The $CH_3Nb(O)H$ and $CH_3Ta(O)H$ molecules can be regarded as being formed via hydrogen transfer from methane to the metal center. Another possible reaction channel is hydrogen transfer to the O atom to form CH_3NbOH and CH_3TaOH. Previous theoretical calculations imply that transition metal monoxides such as PdO can insert into the C−H bond of methane to form CH_3PdOH with an energy barrier of 24.5 kcal/mol.[7,8] A recent study in our laboratory showed that the $OMn(CH_4)$ and $OFe(CH_4)$ complexes underwent photochemical rearrangement to the CH_3MnOH and CH_3FeOH molecules upon ultraviolet irradiation.[12] No evidence was found for the formation of CH_3NbOH and CH_3TaOH in the present experiments. The calculation results showed that the $CH_3M(O)H$ (M = Nb, Ta) molecule is more stable than the CH_3MOH isomer. The CH_3NbOH molecule was predicted to have a $^4A''$ ground state, which is 22.2 kcal/mol higher in energy than the ^2A ground state $CH_3Nb(O)H$ isomer. The CH_3TaOH molecule has a $^2A''$ ground state lying 28.8 kcal/mol higher in energy than the ^2A state $CH_3Ta(O)H$ molecule.

The $O_2Nb(CH_4)$ and $O_2Ta(CH_4)$ complex absorptions also decreased upon broad-band irradiation, during which the $CH_3Nb(O)OH$ and $CH_3Ta(O)OH$ absorptions were produced. This suggests that the $CH_3Nb(O)OH$ and $CH_3Ta(O)OH$ molecules were generated from the $O_2Nb(CH_4)$ and $O_2Ta(CH_4)$ complexes via reactions 7 and 8.

$$O_2Nb(CH_4)\ (^2A') + h\nu \rightarrow CH_3Nb(O)OH\ (^2A) \qquad (7)$$

$$O_2Ta(CH_4)\ (^2A') + h\nu \rightarrow CH_3Ta(O)OH\ (^2A) \qquad (8)$$

According to the CCSD(T)/B3LYP/6-311++G**/SDD calculations, the $CH_3Nb(O)OH$ and $CH_3Ta(O)OH$ molecules are 26.7 and 31.8 kcal/mol lower in energy than the $O_2Nb(CH_4)$ and $O_2Ta(CH_4)$ complexes, respectively. The $CH_3Nb(O)OH$ and $CH_3Ta(O)OH$ molecules can be regarded as being formed via hydrogen transfer from methane to one of the oxygen atoms. Although these isomerization reactions are exothermic, the reactions require activation energy, and the formations of $CH_3Nb(O)OH$ and $CH_3Ta(O)OH$ are photochemical processes.

Conclusions

The reactions of transition metal monoxides (NbO and TaO) and dioxides (NbO_2 and TaO_2) with methane molecules have been investigated using matrix isolation infrared absorption spectroscopy. The metal oxide molecules were prepared by pulsed laser evaporation of bulk Nb_2O_5 or Ta_2O_5 targets. The reaction intermediates and products were identified on the basis of isotopic substitution experiments with $^{13}CH_4$ and CD_4 as well as theoretical calculations. In solid argon, the niobium monoxide molecules reacted with methane to form the $ONb(CH_4)$ complex, which was predicted to have C_{3v} symmetry with the metal atom coordinated to three hydrogen atoms of the methane molecule.

The $ONb(CH_4)$ complex rearranged to the more stable CH_3-Nb(O)H isomer upon 300 nm $< \lambda <$ 580 nm irradiation. The analogous $OTa(CH_4)$ complex was not observed, but the CH_3-Ta(O)H molecule was produced upon UV irradiation. The niobium and tantalum dioxide molecules reacted with methane to form the $O_2Nb(CH_4)$ and $O_2Ta(CH_4)$ complexes, which were predicted to have a $^2A'$ ground state with C_s symmetry. The binding energies for NbO_2 and TaO_2 are larger than those for the corresponding monoxides. The metal dioxide−methane complexes underwent photochemical rearrangement to the more stable $CH_3Nb(O)OH$ and $CH_3Ta(O)OH$ isomers upon ultraviolet irradiation.

Acknowledgment. We gratefully acknowledge financial support from NSFC (20125311 and 20203005) and the NKBRSF of China.

References and Notes

(1) (a) Schröder, D.; Fiedler, A.; Hrusak, J.; Schwarz, H. *J. Am. Chem. Soc*. **1992**, *114*, 1215. (b) Ryan, M. F.; Fiedler, A.; Schröder, D.; Schwarz, H. *J. Am. Chem. Soc*. **1995**, *117*, 2033. (c) Ryan, M. F.; Fiedler, A.; Schröder, D.; Schwarz, H. *Organometallics* **1994**, *13*, 4072. (d) Schröder, D.; Schwarz, H. *Angew. Chem., Int. Ed*. **1995**, *34*, 1973.

(2) Schröder, D.; Schwarz, H. *Angew. Chem., Int. Ed. Engl*. **1990**, *29*, 1433.

(3) (a) Clemmer, D. E.; Aristov, N.; Armentrout, P. B. *J. Phys. Chem*. **1993**, *97*, 544. (b) Chen, Y. M.; Clemmer, D. E.; Armentrout, P. B. *J. Am. Chem. Soc.* **1994**, *116*, 7815.

(4) Aguirre, F.; Husband, J.; Thompson, C. J.; Stringer, K. L.; Metz, R. B. *J. Chem. Phys*. **2002**, *116*, 4071.

(5) (a) Yoshizawa, K.; Shiota, Y.; Yamabe, T. *Chem.−Eur. J*. **1997**, *3*, 1160. (b) Yoshizawa, K.; Shiota, Y.; Yamabe, T. *J. Am. Chem. Soc*. **1998**, *120*, 564. (c) Shiota, Y.; Yoshizawa, K. *J. Am. Chem. Soc*. **2000**, *122*, 12317.

(6) Yoshizawa, K.; Shiota, Y.; Yamabe, T. *Organometallics* **1998**, *17*, 2825.

(7) Broclawik, E.; Yamauchi, R.; Enduo, A.; Kubo, M.; Miyamoto, A. *J. Chem. Phys.* **1996**, *104*, 4098.

(8) Broclawik, E.; Yamauchi, R.; Enduo, A.; Kubo, M.; Miyamoto, A. *Int. J. Quantum Chem.* **1997**, *61*, 673.

(9) Hwang, D. Y.; Mebel, A. M. *Chem. Phys. Lett.* **2002**, *365*, 140.

(10) Hwang, D. Y.; Mebel, A. M. *J. Phys. Chem. A* **2002**, *106*, 12072.

(11) Xu, X.; Faglioni, F.; Goddard, W. A., III. *J. Phys. Chem. A* **2002**, *106*, 7171.

(12) Wang, G. J.; Chen, M. H.; Zhou, M. F. *J. Phys. Chem. A* **2004**, *108*, 11273.

(13) (a) Chen, M. H.; Wang, X. F.; Zhang, L. N.; Yu, M.; Qin, Q. Z. *Chem. Phys*. **1999**, *242*, 81. (b) Zhou, M. F.; Zhang, L. N.; Shao, L. M.; Wang, W. N.; Fan, K. N.; Qin, Q. Z. *J. Phys. Chem. A* **2001**, *105*, 10747. (c) Zhou, M. F.; Zhang, L. N.; Qin, Q. Z. *J. Phys. Chem. A* **2001**, *105*, 6407.

(14) Frisch, M. J.; Trucks, G. W.; Schlegel, H. B.; Scuseria, G. E.; Robb, M. A.; Cheeseman, J. R.; Montgomery, J. A., Jr.; Vreven, T.; Kudin, K. N.; Burant, J. C.; Millam, J. M.; Iyengar, S. S.; Tomasi, J.; Barone, V.; Mennucci, B.; Cossi, M.; Scalmani, G.; Rega, N.; Petersson, G. A.; Nakatsuji, H.; Hada, M.; Ehara, M.; Toyota, K.; Fukuda, R.; Hasegawa, J.; Ishida, M.; Nakajima, T.; Honda, Y.; Kitao, O.; Nakai, H.; Klene, M.; Li, X.; Knox, J. E.; Hratchian, H. P.; Cross, J. B.; Adamo, C.; Jaramillo, J.; Gomperts, R.; Stratmann, R. E.; Yazyev, O.; Austin, A. J.; Cammi, R.; Pomelli, C.; Ochterski, J. W.; Ayala, P. Y.; Morokuma, K.; Voth, G. A.; Salvador, P.; Dannenberg, J. J.; Zakrzewski, V. G.; Dapprich, S.; Daniels, A. D.; Strain, M. C.; Farkas, O.; Malick, D. K.; Rabuck, A. D.; Raghavachari, K.; Foresman, J. B.; Ortiz, J. V.; Cui, Q.; Baboul, A. G.; Clifford, S.; Cioslowski, J.; Stefanov, B. B.; Liu, G.; Liashenko, A.; Piskorz, P.; Komaromi, I.; Martin, R. L.; Fox, D. J.; Keith, T.; Al-Laham, M. A.; Peng, C. Y.; Nanayakkara, A.; Challacombe, M.; Gill, P. M. W.; Johnson, B.; Chen, W.; Wong, M. W.; Gonzalez, C.; Pople, J. A. *Gaussian 03*, revision B.05; Gaussian, Inc.: Pittsburgh, PA, 2003.

(15) (a) Becke, A. D. *J. Chem. Phys*. **1993**, *98*, 5648. (b) Lee, C.; Yang, E.; Parr, R. G. *Phys. Rev. B* **1988**, *37*, 785.

(16) Perdew, J. P.; Wang, Y. *Phys. Rev. B* **1992**, *45*, 13244.

(17) (a) McLean, A. D.; Chandler, G. S. *J. Chem. Phys*. **1980**, *72*, 5639. (b) Krishnan, R.; Binkley, J. S.; Seeger, R.; Pople, J. A. *J. Chem. Phys*. **1980**, *72*, 650.

(18) Andrae, D.; Haussermann, U.; Dolg, M.; Stoll, H.; Preuss, H. *Theor. Chim. Acta*. **1990**, *77*, 123.

(19) Pople, J. A.; Gordon, M. H.; Raghavachari, K. *J. Chem. Phys*. **1987**, *87*, 5968.

(20) Zhou, M. F.; Andrews, L. *J. Phys. Chem. A* **1998**, *102*, 8251.

(21) Green, D. W.; Korfmacher, W.; Gruen, D. M *J. Chem. Phys.* **1973**, *58*, 404.

(22) Weltner, W., Jr.; McLeod, D., Jr. *J. Chem. Phys.* **1965**, *42*, 882.

(23) Brom, J. M., Jr.; Durham, C. H., Jr.; Weltner, W., Jr. *J. Chem. Phys*. **1974**, *61*, 970.

(24) Zhou, M. F.; Dong, J.; Zhang, L. N.; Qin, Q. Z. *J. Am. Chem. Soc*. **2001**, *123*, 135.